W. W. Hansen Experimental Physics Laboratory

STANFORD UNIVERSITY
STANFORD, CALIFORNIA 94305-4085
GRAVITY PROBE B RELATIVITY MISSION

VERIFICATION OF PAYLOAD ON-ORBIT RADIATION ENVIRONMENT COMPATIBILITY

S0610 Rev -

Robert Brumley — 11/29/01
Prepared by: Robert Brumley — **Date**
Payload Technical Manager

11/30/01
Approved by: Bruce Clarke — **Date**
UV Charge Control System RE

11/30/01
Approved by: B. Muhlfelder — **Date**
Program Technical Manager

11/30/01
Approved by: A. Logan — **Date**
Systems Engineer

ITAR Assessment Performed T. Langenstein — 12/5/01 — **ITAR Control Req'd?** ☐ Yes ☒ No
Tom Langenstein

1. Overview

This document verifies the compatibility of the GP-B payload with the on-orbit radiation environment. It completes the formal verification of the PLSE-12 requirement 3.2.5.6.4:

PLSE-12 #	Title	Requirement	Method
3.2.5.6.4	Radiation Environment	The Science Payload shall perform as specified while exposed to on-orbit radiation environment in accordance with Stanford document P0149, "Natural Orbital Environment Specification" section 2.0 titled "Ionizing radiation".	A

For purposes of this document, the GP-B payload consists of the integrated assembly of three major components: the Science Instrument Assembly (SIA), the Science Mission Dewar (SMD), and the flight probe (Probe C). Specifically, this document does not consider the radiation compatibility of the payload electronics. Note that the specification document for each payload electronics box includes the requirement for radiation compatibility, and this requirement is verified in the ADP for each box.

The components of the payload hardware which could conceivably be affected by the on-orbit radiation environment can be divided into four major categories: (1) the science mission gyroscope, (2) the SQUID magnetometers, (3) the telescope Detector Package Assemblies (DPA's), and (4) the fiber optics. Each of these systems is considered separately in the sections below.

2. Science Mission Gyroscopes

The GP-B gyroscopes consist of a fused quartz sphere inside a quartz housing. Various components of the space vehicle have a significant shielding effect which reduces the level of radiation to which the gyroscopes are exposed. The average shielding for each gyroscope is approximately 20 g/cm^2 Al equivalent. The result is that the only component of the on-orbit radiation environment which has a significant impact on the gyroscope are high-energy protons. These protons act to both warm and charge the sphere.

2.1 Gyroscope Charging

Given the proton flux outlined in P0149, high-energy protons charge the rotor at a rate of approximately 1 pC per day during normal non-solar flare conditions. During a solar flare, the rate can increase to 1 pC per hour. This charging results in an increase in the rotor's electrostatic potential.

The change in potential can be calculated according to the equation $Q=CV$, were Q is the net charge on the rotor in coulombs, C is the total capacitance between the rotor and the ground plane and all electrodes (approximately 1000 pF), and V is the rotor potential in volts. The charging rates cited in the above paragraph result in the rotor potential changing at a rate of 1 mV/day in normal conditions, and 1 mV/hour during a large solar flare.

Left uncontrolled, this increase in rotor potential would result in greater electrostatic torques that would result in excess drift of the gyroscope spin axis. Therefore, a special charge control system has been devised to maintain the rotor charge at an acceptable level (less than 10 pC on average). The requirements for this charge control system are called out separately in PLSE-12. Since these requirements are verified separately elsewhere (see the PLSE-12 VRCM), they will not be considered in detail here. However, note that the flight charge control system hardware has already been constructed and meets all requirements. The functionality of the payload component of the charge control system was demonstrated for each gyroscope numerous times (6 times at room temperature and 3 times at low temperature) using procedure P0565. The results of these tests are included in the Payload Test documentation package.

2.2 Gyroscope Warming

This issue has been analyzed in detail in S0495 "Effects of Cosmic Radiation Heating on the Temperature of the Science Gyroscope Rotor". The conclusion is that the gyroscope will stay within the nominal temperature range throughout the mission. See S0495 for details.

3. SQUID Magnetometers

The tests as described in the attached appendix verify the performance of the GP-B flight SQUID in the presence of high energy protons (SQUID III as described in that appendix). These tests confirmed the expected proton-induced, on-orbit flux jump rate in the SQUIDs. Using this flux jump rate for SQUID performance, data reduction simulations demonstrated little impact on overall experiment error. This requirement is contained in PLSE-12 3.7.1.7.2.1.5, which states that on the average there can be less than 1 flux jump every 6 hours.

The data in Figure 1b of Appendix A indicates a total of 9 flux jumps in 200 seconds when the SQUID was exposed to a proton flux of 1×10^5 protons/cm^2/s. Note that the 54 MeV protons used for this experiment have an energy roughly equal to the maximum energy of the on-orbit protons, as documented in P0149. Since the average expected proton flux on orbit is 44 protons/cm^2/s, the expected average number of SQUID flux jumps on orbit is

$$N = \frac{9}{200}\cdot\frac{44}{1\times10^5} = 2\times10^{-5} \text{ flux jumps/s} = 1 \text{ flux jump every 14 hours}$$

This meets the required flux jump specification by better than a factor of 2. Furthermore, it is expected that the on-orbit flux jump rate will be significantly better than what was observed in this test. The reason for this is that the magnetic field will be lower on-orbit than it was for these tests and also, the thermal grounding of the SQUIDs in the flight configuration is superior to the grounding used in these tests. Therefore, the flight SQUIDs will fully meet the program requirements in the presence of high energy particles.

4. DPA's

A cryogenically cold DPA in operational mode with TRE attached was irradiated by the University of California at Davis Cyclotron with 35-70 MeV protons. Details of this test are

recorded in S0611. The beam was generated at a low intensity such that the number of hits on an individual Si photodiode were observed to range from less than one per 100 ms integration period (ramp) to several hundred per ramp. No irreversible degradation in DPA performance was observed.

An engineering prototype DPA was used that contained all active elements of the Flight like DPA's: Si photodiodes, Si JFETs, capacitors, resistors, and heaters that were bonded using the techniques of the flight detectors.

Data were recorded and archived. A typical ramp displays a slope in output signal with increasing time that is smooth or noisy depending on the light signal with which it was illuminated. Occasionally there is a step function apparent in the slope. The values of the ramp's slopes before and after the event are identical within the measurement errors. There are no discernable time constants associated with the step function either prior or subsequent to the event. There appear to be a spectrum of step heights for radiation events observed during testing suggesting that the photodectectors also serve as ionizing radiation detectors that respond proportionally to the deposited radiation energy.

The results indicate that the on-orbit radiation will occasionally cause a step in the output of the DPA's. No permanent damage was observed. This behavior is easily accommodated in software and does not reduce the overall performance of the payload. The verification of the integrated payload/spacecraft/software performance will occur at the space vehicle level and is not addressed here.

In conclusion, the DPA's response to the on-orbit radiation environment has been demonstrated experimentally and documented in S061, and no damage was observed. The DPA's have been experimentally verified to be compatible with the on-orbit radiation environment.

5. Fiber Optics

Optical fibers from the same lot that are used in the flight probe and gyroscopes were irradiated with high-energy protons at the University of Davis cyclotron. The purpose of this set of experiments was to evaluate the effect that on-orbit radiation will have on the optical fiber transmittance. This transmittance in the operational band of 254 nm was measured prior to, during, and after the exposure to the radiation.

The anticipated flux of high-energy protons on orbit is approximately 44 protons/cm^2/s, with a total flux over the course of a year of 1.4×10^9 protons/cm^2. Two different tests were performed on the same optical fibers. In the first, the fibers were exposed to lower-energy (2-7 MeV) protons at fluxes of 10^5, 10^6, and 10^7 protons/cm^2/s, with a total irradiation of approximately 5.4×10^{10} protons/cm^2. This is almost 40 times the total expected on-orbit dosage. In the second experiment, the fiber was irradiated at 60 MeV for one hour at a flux of 10^6 protons/cm^2/s, with a total exposure of 3.6×10^9 protons/cm^2 (2.6 times the total expected on-orbit dosage). Note that 60 MeV is the highest energy present in the on-orbit radiation environment in any sizable quantity (see P0149 for details). Therefore the second experiment was equivalent to flying 2.6 missions with all radiation being concentrated at the highest levels.

The UV fibers in the GP-B experiment are made of high-quality quartz. The effect of radiation on the transmittance of quartz is well known, allowing a high-confidence predictions of the experimental results. Changes in quartz transmittance due to radiation has two components. The first involves the creation of a metastable "color center" which temporarily darkens the quartz. This color center is not stable, and a self-annealing process in the quartz removes the color center, regaining the original transmittance. The second damage mechanism, which is present only for proton energies greater than approximately 10 MeV, results from interactions with the nuclei in the quartz and can lead to impurities that result in permanent degradation of the fiber.

Figure 1 shows the results from the first experiment. Since the protons flux was approximately 10^5 times greater than is expected on orbit, the creation of color centers occurred at a much greater rate than the self-annealing process, allowing the creation of the metastable color centers to be observed. On orbit, the lower proton flux means that the self-annealing process will dominate, resulting in no observable degradation of the transmittance due to this mechanism.

However, Figure 1 does display some permanent degradation. The total permanent drop in transmittance is approximately 7%. Since this was after exposure to approximately 40 missions worth of low-energy protons, this is equivalent to a drop of approximately 0.2% per mission, which is negligible. Note that even if the self-annealing process were not to happen, the total drop in fiber transmittance expected in a mission would still be only 1%, which is also negligible.

The results of the second experiment in which the fiber was bombarded with high-energy 60 MeV protons show a similar pattern. In that case, the total permanent fiber degradation after an exposure equal to 2.6 missions in which all radiation is concentrated at the high-energy end of the spectrum was 2.3% (0.9% drop per mission), which meets all requirements.

In conclusion, samples of the fiber optics taken from the same lot as the flight cables were exposed to both low and high-energy radiation. The fibers were irradiated to levels significantly in excess of the expected flight levels. In all cases, the total drop in transmittance per mission was less than 1%, which is well within acceptable boundaries. Therefore the probe and gyroscope optical fibers are compatible with the on-orbit radiation environment.

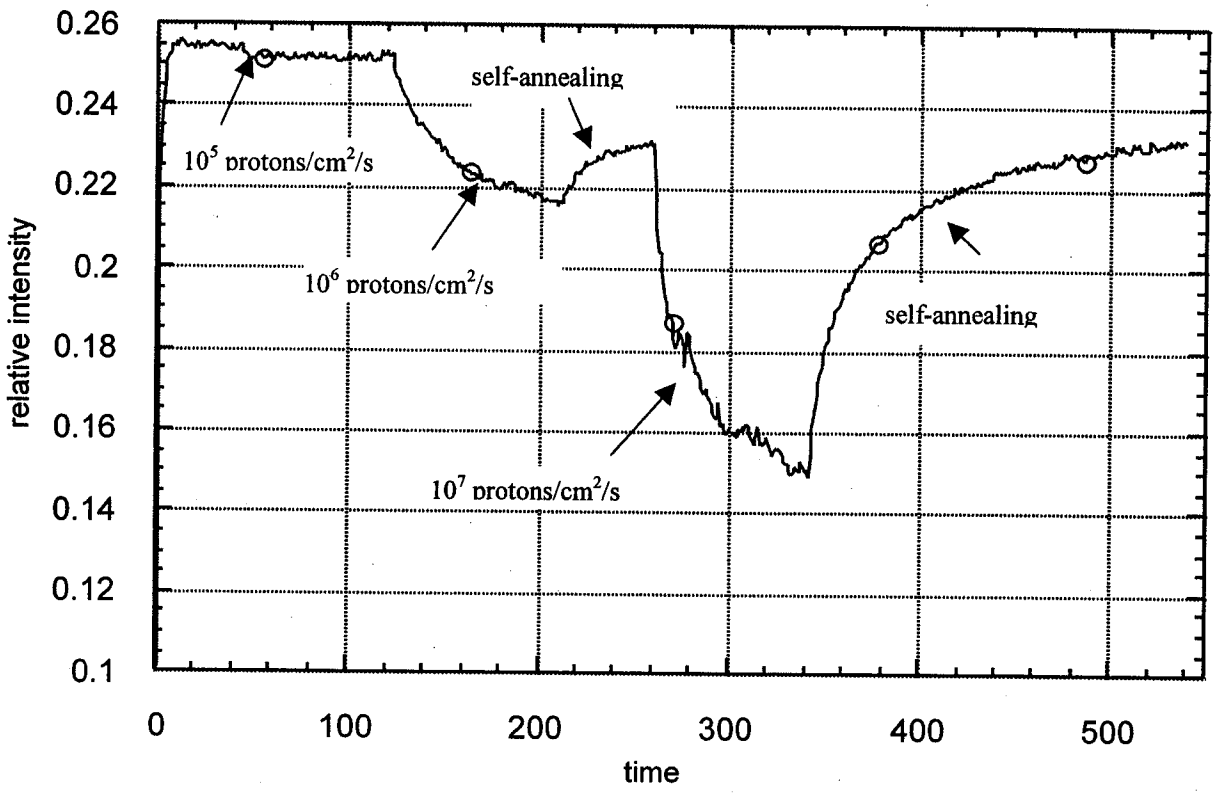

Figure 1: UV transmittance of optical fiber for various proton fluxes

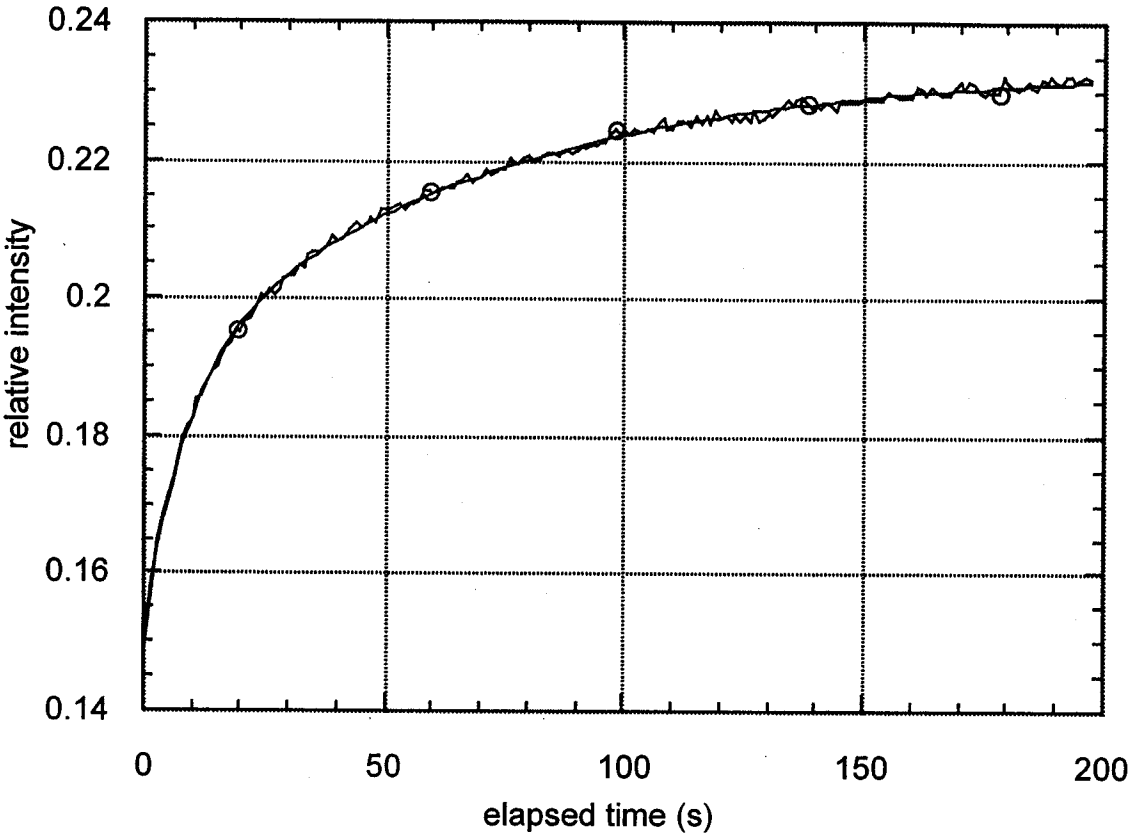

Figure 2: Recovery curve at completion of proton irradiation (final 200 seconds from Figure 1)

Appendix: Effects of High Energy Proton Bombardment (50-280MeV) on dc SQUIDS

B. Muhlfelder, G. M. Gutt, J. M. Lockhart†
Hansen Experimental Physics Laboratory, Stanford University, Stanford, California 94305

P. Carelli
Universita' dell'Aquila, L'Aquila, Italy

A. Zehnder, F. Mattenberger, W. Hajdas, Ph. Lerch, R. Henneck
Paul Scherrer Institute, Villigen, Switzerland

†Also with Dept. of Physics and Astronomy, San Francisco State University, San Francisco, California

***Abstract*—Three thin film dc SQUIDs of varied construction were bombarded with energetic protons in the energy range of 50 to 280 MeV. Measurements of the voltage output of the dc SQUIDs were taken in open loop, as well as flux locked mode, in an environment of proton flux that was varied from 10^4 to 10^7 protons/cm^2/s. Discrete voltage jumps corresponding to 0.01 to 0.001 flux quanta were observed in two of the three SQUIDs in the flux locked mode; discrete changes in the open loop SQUID output voltage were also observed. Some data appear to be consistent with proton-induced flux motion in the body of the SQUID loop.**

I. INTRODUCTION

SQUIDs (Superconductive Quantum Interference Devices) are known to be ultra-sensitive detectors of magnetic flux. Many precision experiments such as the relativity gyroscope experiment, the satellite test of the equivalence principle, and inductive type monopole detectors make use of these devices [1]-[3]. In general, such experiments require very stable magnetic field environments. It has been proposed that energetic particles can drive small volumes of a superconductor into the normal state, thereby inducing magnetic flux motion [4]. In space-based experiments, it is well known that there are situations (such as the South Atlantic Anomaly and solar flare events) in which energetic protons are common [5]. In addition, cosmic protons of ultrahigh energy are known to be incident on the earth's surface. To date, there have been only limited studies on the interaction between high energy protons and superconductive systems [4], [6], [7]. In this paper we report on the measured interactions between high energy protons and dc SQUIDs.

II. EXPERIMENTAL APPARATUS

Three dc SQUIDs of varied construction were tested in this experiment. The first was manufactured by the National Institute of Standards and Technology (NIST), Boulder, CO. The second was manufactured at the Istituto di Elettronica dello Stato Solido of C.N.R., Rome, and the third device was fabricated by Quantum Design, Inc., San Diego, CA. Henceforth we refer to these devices as SQUIDs I, II and III.

TABLE I
Relevant physical and electrical properties of the three SQUID sensors.

ATTRIBUTE	SQUID I	SQUID II	SQUID III
Josephson Junction Area (m^2)	6.1x10^{-12}	4x10^{-12}	7.1x10^{-12}
Silicon Substrate Crystal Orientation	<100>	<111>	<100>
Junction Type	Nb/AlO/Nb	Nb/NbOx/Pb InAu	Nb/AlO/Nb
SQUID Loop Area (mm^2)	0.36	1.3	2.1
SQUID Hole Area (mm^2)	2.5x10^{-3}	0.14	0.017
Loop Material and Thickness (nm)	PbInAu 550	Nb 300 PbInAu 430	Nb 120
SQUID Critical Current (μA)	18.1	38	10
Carrier Material	Sapphire	Sapphire	Fiberglass
B Field at SQUID (μT)	0.2	40	0.2

Table I gives some of the characteristics of the devices.

The devices were operated in vacuum and therefore required a thermally conductive path to the liquid helium bath to allow adequate cooling. The sapphire carriers of SQUIDs I and II were connected to the dewar's cold plate using copper braiding. SQUID III was thermally grounded by connecting its input coil to thermal ground with electrically insulated copper wire. We believe that the thermal grounding of SQUIDs I and II was better than that of SQUID III. All of the SQUIDs were isolated from fluctuations in the external magnetic field by using niobium cans. SQUIDs I and III and their associated niobium cans were then placed within ferromagnetic shields. SQUID II had no ferromagnetic shield. The SQUID's input coils (of order 1μH) were left open circuit to eliminate input coil persistent currents. The experimental configuration allowed us to operate and monitor the simultaneous performance of the three SQUIDs in the presence of proton bombardment.

The experiment was performed at the Paul Scherrer Institute in Villigen, Switzerland, using the proton irradiation facility (PIF). The proton energies were adjusted to 54 MeV and 280 MeV using aluminum plates as degraders. Proton flux was varied by reducing the total beam intensity. The beam was collimated to an area of 2 cm by 6 cm by an Fe collimator and was homogeneous over this area to ±10%. The SQUIDs were oriented approximately normal to the proton beam. The configuration allowed simultaneous proton

bombardment of all three SQUIDs. On-line monitoring of the flux was provided by observing single

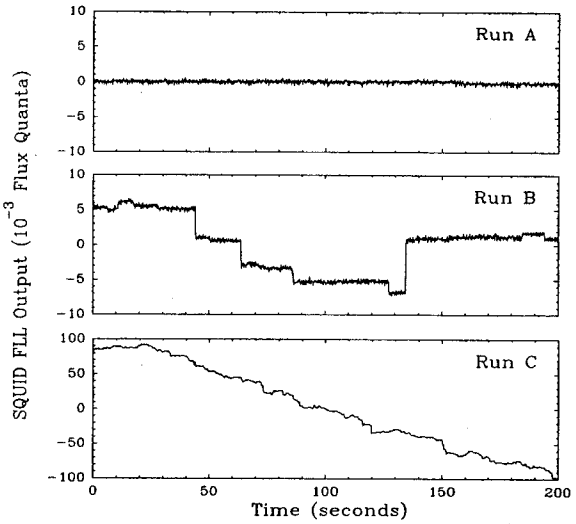

Fig. 1. SQUID III FLL time series output. Run A, no incident protons. Run B, 54 MeV protons with a flux of $1x10^5$ p/cm^2/s. Run C, 54 MeV protons with a flux of $1.6x10^6$ p/cm^2/s.

proton events in a small (1x1x1 mm^3) plastic scintillator in front of the cryostat.

The effects of spurious electromagnetic interference were tested by moving the SQUIDs out of the immediate path of the proton beam. In this test, no observable change was detected in the SQUIDs' output when the beam was cycled on and off at the maximum beam current. The control electronics for the SQUIDs was placed outside the beam during these measurements.

The SQUID temperatures were monitored with two germanium resistance thermometers (GRTs). Based upon our calculations we expected the maximum power deposited into each of the SQUIDs (at a proton flux of 10^7 p/s/cm^2) to be approximately 50 pW, the power deposited into each silicon substrate at this flux to be approximately 200 nW, and the power deposited into each of the niobium cans to be approximately 50 μW. Although we did not expect to see a temperature rise resulting from the absorption of this amount of power, the GRTs did show an apparent instantaneous temperature increase of 5 mK. It is well known that particle bombardment produces electron-hole pairs in semiconductor devices. We attribute the apparent change in temperature to this effect and believe that the actual, proton-induced temperature rise was less than 1 mK.

III. RESULTS

The SQUIDs were operated using conventional flux locked loop (FLL) electronics to linearize the flux to output voltage transfer function. The proportionality factor for each of the three SQUIDs was of order 1 V/Φ_0 (where V is the output voltage of the SQUID electronics and where Φ_0 is the flux quantum, $2.07x10^{-15}$ Wb). The SQUID flux power spectral densities, S_Φ, for each of the three SQUIDs with no incident protons is given in Table II. Note that there were significant differences in the noise performance of the three SQUIDs. The low frequency noise performance of SQUID I and the overall noise performance of SQUID II were inferior to our typical laboratory results. We believe that elevated SQUID temperatures may account for the inferior noise performance (the SQUIDs were operated at approximately 6 K). In any case, all of the SQUIDs functioned in a stable manner, allowing us to set a minimum detectable level for potential interactions between the SQUIDs and high energy protons.

TABLE II

Noise performance of the three flux locked SQUIDs at a temperature of 5.6 K with no incident protons. Similar results were obtained at 6.3 K.

Attribute	SQUID I	SQUID II	SQUID III
S_Φ @ 100 Hz (Φ_0^2/Hz)	$6x10^{-11}$	$3x10^{-9}$	$1x10^{-10}$
S_Φ @ 1 Hz (Φ_0^2/Hz)	$2x10^{-9}$	$3x10^{-9}$	$2x10^{-10}$
1/f Noise Knee (Hz)	30	<1	1

The three SQUIDs had varied responses to proton bombardment. SQUID III showed significant output voltage jump events for proton fluxes of 10^5 p/cm^2/s and higher. Fig. 1 gives time series data for SQUID III for three different proton flux densities at an energy of 54 MeV. The frequency of events in the time domain was approximately proportional to the proton flux. The time of transition for each individual jump exceeded the 10 Hz sampling rate of our data acquisition system. SQUID II showed qualitatively similar behavior to SQUID III. SQUID I showed no response to proton bombardment at any flux or energy. No temporal correlation of events was observed between SQUIDs II and III. The observed effects for SQUIDs II and III also varied with proton energy. Both the frequency as well as the amplitude of jumps appeared to be approximately five times larger for the 54 MeV protons than they were for the 280 MeV protons. We note however, that the SQUID temperature was 6.3 K for the 54 MeV run and was 5.6 K for the 280 MeV run. In both cases the SQUID temperatures were held constant to 20 mK.

Fig. 2 shows time domain data acquired before, during and after proton bombardment of SQUID III. Several observations are in order:

1. At the completion of proton bombardment, the SQUID output voltage did not return to its prebombardment value.
2. The response to the protons was faster than our sampling frequency of 10 Hz. This applied at both points A and B.
3. In general, there appeared to be a preferred direction to the drift in the SQUID output (see also Fig. 1, Run C.)

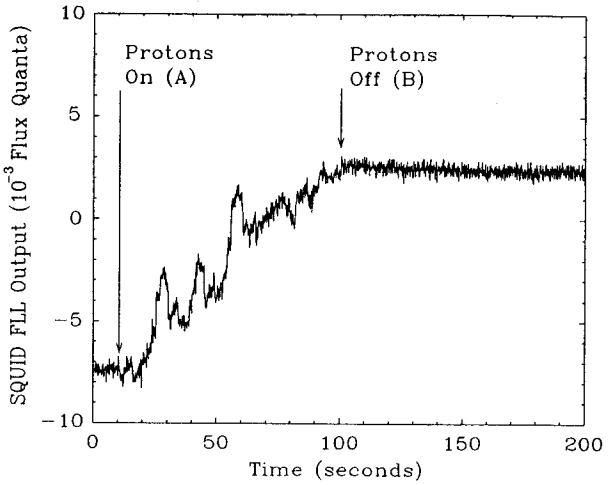

FIG. 2. SQUID III FLL time series output. 280 MeV protons with a flux of $6x10^7$ p/cm^2/s.

In a second set of experiments, the feedback flux was disabled, allowing us to observe more directly the behavior of the SQUID. The SQUID voltage signal resulting from FIG. 2. SQUID III FLL time series output. 280 MeV protons with a flux of $6x10^7$ p/cm^2/s.

the application of a flux modulation signal of amplitude $\Phi_0/4$ was observed on an oscilloscope. This signal is affected by the average magnetic flux state of the SQUID and, in a different way, by changes in the critical current of the SQUID junctions. Flux changes of 10^{-2} Φ_0 and larger could be detected, as could critical current changes of 0.2 μA or greater.

We observed large, discrete changes in the above signal for SQUIDs II and III during bombardment with 54 MeV protons. These signal changes were of the type expected from changes in the average flux state of the SQUID and were consistent with the amplitude of the signals observed in the flux-locked mode. It was further found that the SQUID signal observed at the conclusion of proton bombardment could be restored to its prebombardment form by applying a dc magnetic flux to the SQUID.

No changes of the type to be expected from critical current variations were observed, nor was any permanent damage noted in the SQUIDs.

IV. DISCUSSION

We believe that thermally induced flux motion in the body of the SQUID loop is the best explanation for the data which has been presented here. Our numerical simulations indicate that a small volume of superconductor is driven into the normal state each time a proton passes through the SQUID loop material. When such a proton passes sufficiently close to a magnetic flux line, the material surrounding this line would be driven into the normal state. This event would allow the trapped flux line to move, thereby causing a jump in the SQUID output. A thermal diffusion model was used to predict the cross-sectional area which was driven normal for each incident proton. For SQUID III, we expected this area to be 0.054 μm^2 for each 280 MeV proton. The corresponding area for each 54 MeV proton was 0.18 μm^2. For this SQUID, the trapped magnetic flux density was approximately 10^4 Φ_0/cm^2. For this trapped flux level and 54 MeV protons incident on this SQUID at a flux of 10^5 p/cm^2/s, we expect direct heating of a magnetic flux pinning site about every 30 seconds. This calculation is in good agreement with the data (see Fig. 1, Run B). It has been suggested that the preferred direction of SQUID voltage drift exhibited in Fig. 1, Run C and in Fig. 2 might be explained by a unidirectional Lorentz force caused by the dc bias current flowing through the SQUID [8].

Our understanding of the data is not complete. Based upon the explanation as given above, one would have expected flux movement in all three SQUIDs. Since SQUID I did not show such behavior, we are attempting to isolate its unique properties. For the observed effects in SQUIDs II and III, we have not completely ruled out nonthermal mechanisms such as charged particle interactions at the band and atomic level. However, if our flux motion explanation is correct, then the implications of this behavior may extend to many superconductive systems which rely on stable magnetic field environments. Experiments are in progress to better understand the overall results reported here.

ACKNOWLEDGEMENTS

We wish to thank B. Parkinson and C.W.F. Everitt for suggesting this experiment. In addition we would like to thank the following for their useful discussions and efforts: B. Cabrera, D. Yon and T. Ale. We would also like to thank M.W. Cromar, M. G. Castellano and Quantum Design, Inc., for SQUID support and the group of P. Martinoli for use of their spectrum analyzer. This work has been funded under NASA Contract #NAS8-36125.

REFERENCES

1. J.P. Turneaure, C.W.F. Everitt, B.W. Parkinson, D. Bardas, J.V. Breakwell, S. Buchman, W.S. Cheung, D.E. Davidson, D.B. DeBra, W.M. Fairbank, S. Feteih, D. Gill, R. Hacker, G.M. Keiser, J.M. Lockhart, B. Muhlfelder, R.T. Parmley, Xinhua Qin, M.A. Taber, R.A. Van Patten, Y.M. Xiao, and P. Zhou, Adv. Space Res. 9, 29 (1989)
2. P.W. Worden, Acta Astronautica 5, 27 (1978)
3. B. Cabrera, Phys. Rev. Lett. 48, 1378 (1982)
4. J.F. Ziegler, C.C. Tsuei, C.C. Chi, C.D. Tesche, and P. Chaudhari, Physical Review D 28, 1793 (1983)
5. T.J. Sherrill, Sky & Telescope, p. 134, Feb. 1991
6. S. King, R. Magno, and W.G. Maisch, IEEE Trans. Nuc. Sci. 28, 1359 (1991)
7. R. Mango, R. Shelby, M. Nisenoff, A.B. Campbell, and J. Kidd, IEEE Trans. Mag., 19, 1286 (1983)
8. Private communication with B. Cabrera.